



# Pool boiling heat transfer characteristics of graphene-based aqueous nanofluids

Amir Akbari<sup>1</sup> · Seyed Ali Alavi Fazel<sup>1</sup> · Sarah Maghsoodi<sup>1</sup> · Amirhossein Shahbazi Kootenaee<sup>1</sup>

Received: 3 February 2018 / Accepted: 8 March 2018 / Published online: 19 March 2018  
© Akadémiai Kiadó, Budapest, Hungary 2018

## Abstract

In the present study, experiments on pool boiling heat transfer of graphene nanofluids on a flat heater surface (40 mm diameter) were conducted under the saturated boiling and atmospheric pressure. This study also examined the thermal conductivity behavior of nanofluids based on graphene and functionalized graphene (PEG-graphene). The characteristics of pool boiling heat transfer such as boiling heat transfer coefficient (HTC), critical heat flux (CHF) as a function of heat flux and mass fraction of graphene sheets water-based graphene nanofluids have been measured and discussed. In addition, effective thermal conductivities versus temperatures for different concentrations of graphene were determined. From the boiling experimental results, it was indicated that the enhancement of boiling HTC and CHF changes considerably via increasing the concentration of graphene sheets. The results demonstrated that at the same temperature and concentration, thermal conductivity of nanofluid including PEG-graphene was significantly higher than that of one including pure graphene. In PEG-graphene/water nanofluids, CHF increased as the concentration increased. The results indicated that the enhancement in CHF was above 72% at the concentration of 0.1 mass%. The results demonstrated that PEG-graphene nanofluids at all concentrations (0.01, 0.05 and 0.1 mass%) have a suitable dispersion and fewer tendencies for agglomeration and precipitation, compared to graphene without functionalization.

**Keywords** Pool boiling · Critical heat flux · Boiling heat transfer · Graphene · Functionalization

## Introduction

Among the three heat transfer methods, liquid–vapor phase change heat transfer, known as boiling heat transfer, is the most efficient because latent heat has a high capacity [1, 2]. Boiling heat transfer is utilized in a variety of industrial processes such as refrigeration, steam generation, cooling of electronic chips, various chemical processes, solar thermal direct steam generators, pressurized water reactors and nuclear reactor cooling. Pool boiling is also a complex heat transfer process because it is affected by a number of different factors, including heating modes (constant wall heat flux or constant wall temperature), thermal characteristics of vapor and liquid phases, size, orientation and surface properties of the heater (contact angle and surface

microstructures), heating conditions (increased or decreased wall heat flux or wall temperature) and saturation temperatures [3].

Low thermal conductivity of conventional heat transfer fluids such as air, (DW) deionized water, ethylene glycol (EG) and engine oil is one of the greatest problems in high heat transfer applications in mechanical equipment and engineering processes. Adding ultrafine solids particles suspended in the base fluid could improve thermal conductivity of fluids. The early studies showed that the poor dispersion stability of suspended particles with sizes in the range of millimeters or micrometers could affect adversely on effective thermal conductivity. Their low stability suspension results in abrasion and channel clogging. However, it was recently known that nano-sized particles (1–100 nm) suspensions in a common fluid can lead to more stable and high thermal conductivity as well as enhanced rheological properties. The term ‘nanofluid’ was first suggested by Choi in 1995 [4]. Many studies have indicated an increased interest in nanofluids in order to enhance heat transfer,

✉ Seyed Ali Alavi Fazel  
s.alavifazel@yahoo.com

<sup>1</sup> Department of Chemical Engineering, Mahshahr Branch, Islamic Azad University, Mahshahr, Iran

stability and thermophysical properties and performance [5–15].

A nanofluid is a suspension containing nanometer-sized particles such as metals, oxides, carbides or carbon nanostructures. Because of superior thermal and mechanical properties as well as chemical stability, among different carbon nanostructures graphene and carbon nanotubes (CNT) are promising additives for future heat transfer equipment [16, 17]. Graphene has attracted significant attention from the research community when Geim and Novoselov [18] demonstrated that a two-dimensional honeycomb monolayer is formed by graphene. There has been much interest recently in graphene, which has a single layer of carbon atoms in a hexagonal lattice, due to its extreme electrical and thermal properties [1]. Because of high specific surface area, superior thermal conductivity and good stability in the presence of covalent and non-covalent functionalization, graphene-based materials have attracted many researchers throughout the world [19, 20]. However, a main problem that should be addressed for graphene before its applications is poor dispersibility in common organic and inorganic solvents [17, 21]. Sometimes good dispersion of graphene in common solvents is an important step toward the formation of homogeneous nanocomposites. So modification of graphene to alter its solubility is critical for different commercial applications. Graphene can usually be altered by covalent and non-covalent methods. Non-covalent methods involve  $\pi$ - $\pi$  stacking interactions, electrostatic interaction, hydrogen bonding, coordination bonds and van der Waals force [8, 21, 22]. This modification method can maintain the natural structure of graphene to a maximum extent; however, there are comparatively poor interactions between functionalities and graphene surface, so it is not proper for some applications involving strong interactions. Covalent methods can be employed for creating the composites with strong interactions between graphene and the modifier [23]. Functionalization of graphite covalently by oxidizing with  $\text{KMnO}_4/\text{NaNO}_3$  mixture in concentrated  $\text{H}_2\text{SO}_4$  using Hummer's method followed by ultra-sonication can yield bulk quantities of GO (graphene oxide) [23, 24], and chemical reduction using hydrazine hydrate/ $\text{NaBH}_4$  or thermal reduction [25] (at 950 °C in inert atmosphere for 10 s) creates rGO (reduce graphene). The GO has sufficient amount of hydroxyl, epoxy and carboxyl groups so it is of hydrophilic nature which makes it incompatible with most hydrophobic polymers [26]. The above-mentioned functional groups of GO provide opportunity for functionalizing chemically with polymers, but rGO does not have sufficient functionality for this end. Therefore, chemical attachment with small molecule having functional groups leads to sufficient functionality which facilitates both GO and rGO for giving considerable opportunities for more

modification with polymer either by 'grafting to' or by 'grafting from' techniques.

On the other hand, there are two critical issues during boiling heat transfer, performance (boiling heat transfer coefficient) and critical heat flux (CHF), which describes the limit of boiling heat transfer in a thermal system. In CHF phenomena, the surface is covered by a vapor film so that the liquid supply for cooling is prevented [27–29]. This results in an increase in thermal resistance, so that the surface temperature is increased rapidly leading to the system failure such as a severe accident in a power plant. So it is important to understand CHF phenomena which may improve efficiency and safety margins. There have been several reports of predicting CHF phenomena [30–33] and methods of enhancing CHF (i.e., extend the nucleate boiling regime) [29]. Recently, it has been tried to increase the critical heat flux (CHF) during boiling heat transfer by using graphene colloidal suspensions, since its synthesis for mass production of graphene was reported. Thermo-physical characteristics of working fluids play an important role for improving heat transport. However, weak thermal characteristics of conventional heat transfer fluids restrict the system performance, particularly for graphene nanoparticles, because it is new and there is not sufficient information about it in different conditions.

The present study aimed to investigate the heat transfer coefficient and the critical heat flux during the nucleate pool boiling of deionized water on a stainless steel surface in the existence of nanoparticles of graphene and functionalized graphene and the characteristics of the nanofluids were reported.

## Experimental

### Materials and methods

The experimental study on nanofluids involves the preparation method that should be agglomeration free and less deposition in long term in real applications. Nanofluids are composite materials of liquid (base fluid) and solid (nanoparticle) and need some fundamental requirements such as durable stable suspension, negligible agglomeration of nanoparticles, no chemical change of the base fluid (acidic), etc. [8, 21, 22]. Nanofluids are developed by dispensing nano-sized particles in the base fluid such as water, oil, ethylene glycol (EG) and usually are produced by a single (e.g., graphene oxide) or two-step (e.g., GNP nanofluid) preparation method [34, 35].

Deionized water and graphene nanoplatelets (diameter of 1–20  $\mu\text{m}$ , thickness of < 40 nm) employed in the present research were supplied by Vira Carbon Nano Materials (VCN Materials Co.), and the base fluid used was

deionized water (DI). Aluminum chloride, hydrochloric acid, dimethylformamide were bought from Merck, Ind.

In this study, graphene nanofluids with mass concentration of 0.01, 0.05 and 0.1% were used and a two-step method was employed. First graphene nanoplatelets (GNP) with the specified mass percentages mixed up on a base fluid (DI) in order to obtain a stable and uniform suspension. The samples were then placed in the ultrasonic bath (60 kHz, 200w, 4 L Capacity) for 2 h. The samples specifications are shown in Table 1.

Due to low dispersivity of pristine GNP in deionized water, gum Arabic (GA) was used as the non-covalent group with a ratio of 1:1 [36]. So selection of an appropriate surfactant with proper concentration in order to enhance thermal properties with no influence on dispersion stability is recommended [17, 36]. In the second phase, the method of functionalization with covalent groups was used, all the details of which are explained in the next section. Covalent modification of graphene is extremely favorable if stronger interaction between graphene and the modifier is needed. However, it is usually difficult to recognize as the ideal graphene does not have functional groups that can be conjugated with. In this case, it is possible to realize the covalent modifications through disruption of the conjugation of graphene sheets, resulting in the compromising of its natural conductivity. This method is interesting if other properties of graphene are demanded. Direct doping heteroatoms onto the graphene lattice is another way of realizing covalent modifications [21].

As can be seen in Table 1, samples of 1–3 and 4–6 are GNP/DW and functionalized GNP with PEG/DW, respectively.

### Functionalization of graphene

Owing to desired thermal properties such as high conductivity, graphene is a promising material; however, poor dispersivity in most of solvents has restricted its applications because of effective van der Waals interactions [30]. Functionalization has been employed as a method which is capable to tackle the problem of poor interaction of graphene. Consistent with the prior studies, covalent functionalization and non-covalent functionalization were

considered as two effective techniques to develop the dispersion of graphene in different solvents. To solve the problem, the liquid-phase exfoliation of graphite in the presence of high surface tension organic solvents, accompanied by continuous sonication, was suggested as a new technique to produce single-layered and/or few-layered sheets of graphene. However, since there are not easily miscible functional groups, such as polymers to reduce interlayer attractions, there is a tendency for the graphene sheets suspended in the high surface tension base fluids tend to be aggregated. Also, a stable dispersion in base fluids cannot be achieved for liquid-phase exfoliated graphene because there are considerable  $\pi$ - $\pi$  interactions, suggesting high level of aggregation. Another new method is liquid-phase exfoliation of graphite which develops high-quality graphene without structural defects. Nevertheless, the exfoliation performances of the majority of the solvents proposed in previous attempts were very low because of lack of graphene solubility [8, 22]. On the other hand, it sometimes occurred that the samples obtained are exfoliated to a limited extent and still have extensive domains of stacked graphitic layers. In order to improve the efficiency of exfoliation by this technique, the chemical functionalization of graphite with different functional groups, such as 4-bromophenyl, offers a new way to enhance its solubility in polar, aprotic, organic solvents, so that there will be less problems with the exfoliation of bulk graphite [20, 37]. The functionalization procedure for the synthesis of PEG-treated GNP follows the method explained by Amiri et al. [20, 37]. In this study, the pristine GNP (10 mg) and  $AlCl_3$  as a Lewis acid (184.5mg) were poured into an agate mortar and were grounded for several minutes. Then this mentioned mixture and 10 mL PEG were poured into a Teflon vessel and sonicated for 30 min at 50 °C until a homogeneous suspension was obtained.

Next, the addition of 0.5 mL concentrated hydrochloric acid was performed drop by drop with sonication at 50 °C. Then in an industrial microwave (Milestone Micro SYNTH programmable microwave system), the mixture was heated up to 120 °C with output power of 700 W for 30 min. Upon completion of the reaction, the resulting mixture was left to be cooled to the room temperature and filtered through a thin layer Teflon membrane. The filter cake was

**Table 1** Specification of the graphene nanofluid samples

Samples number	Nanofluid mass percentage	Mass percentage graphene	Deionized water
1	GNP/deionized water	0.01	99
2	GNP/deionized water	0.05	95
3	GNP/deionized water	0.1	90
4	GNP-PEG/deionized Water	0.01	99
5	GNP-PEG/deionized Water	0.05	95
6	GNP-PEG/deionized Water	0.1	90

carefully washed with dimethylformamide DMF and abundant deionized water in order to eliminate any unreacted materials and then dried under vacuum at 50 °C. Figure 1 indicates the Schematic processes.

## Characterization

### SEM Scanning electron microscope

Figure 2 shows scanning electron microscope (SEM) images of the pristine GNP. As can be seen in Fig. 2, a transparent large area could be recognized on graphene sheet with wrinkles on the surface and folding at the edges of graphene sheets. Therefore, wrinkles and cracks can be easily observed on the point (a) indicating the formation of folded structure of graphene. Such pattern is resulted from the presence of low layer structures of graphene sheets. Spot (b) in Fig. 2 indicates the formation of few-layered graphene because of transparency, while point (c) shows multilayer graphene sheets with limited distribution according to SEM image [20, 37].

On the other hand, there was not observed any signal of functionalized groups on the surface of graphene nanofluids.

### Tem

Transmission electron microscopy (TEM) was used in order to determine the characteristics of surface morphology/structure of GNP nanofluids. Figure 3 indicates TEM images of GNP functionalized with PEG taken by HITACHI TEM system E.A. FISCHIONE Instruments, Inc. at 120 kV. To measure TEM, the dispersion of graphene nanosheets in absolute ethanol via mild ultra-sonication was performed. The graphene nanofluid was prepared by the dispersion of graphene/functionalized graphene (with PEG) nanoparticles into deionized water as a base fluid.

For the analysis of size and morphology of the nanoparticles, a high-resolution transmission electron

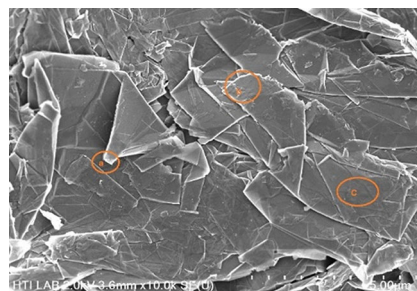


Fig. 2 SEM image of the pristine graphene nanoplatelets

microscopy (HRTEM) was employed. Figure 3 indicates nanoplatelets of graphene dispersed in the base fluid of deionized water and its diffraction pattern. Even following 2 h of ultrasonic vibration, these nanoplatelets were dispersed evenly in deionized water.

### FTIR spectroscopy

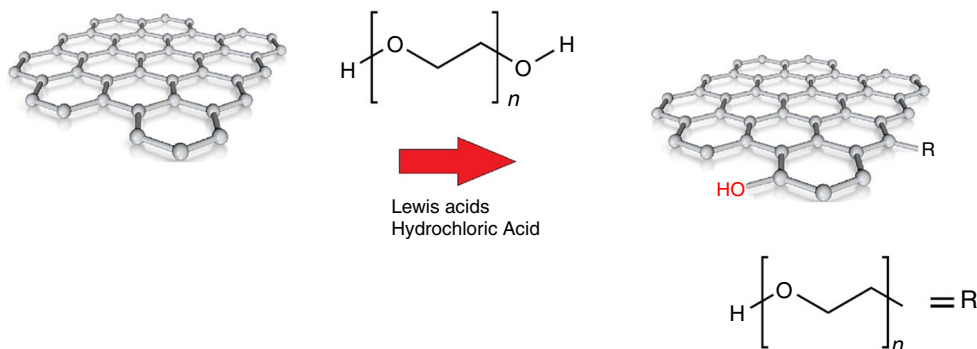
To identify the functionalization and chemical structure of pristine graphene and PEG-functionalized graphene, Fourier transform infrared or FTIR was utilized (Thermo Scientific, Nicolet 6700). The FTIR spectra of the GNP and PEG-graphene are shown in Fig. 4.

Usually 1750 scans over the range 500–4000  $\text{cm}^{-1}$  are taken for each sample with a resolution of 2  $\text{cm}^{-1}$  and summed up to provide the spectra. It was observed that the FTIR spectrum of pristine graphene did not provide any evidence of PEG [20]. There are no strong peaks associated with any functional groups in the FTIR spectrum of pristine graphene [24], and the peak at 1493  $\text{cm}^{-1}$  can be attributed to C=C banding vibrations of aromatic structures [23, 38].

There were multiple peaks in the range of 500–4000  $\text{cm}^{-1}$  for FTIR spectrum of PEG-graphene. In graphene upon modification with PEG, several new bands at 834, 1082, 1416, 2934 and 3270  $\text{cm}^{-1}$  were seen.

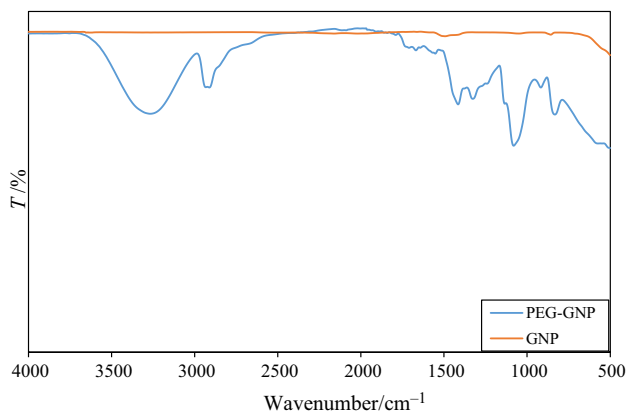
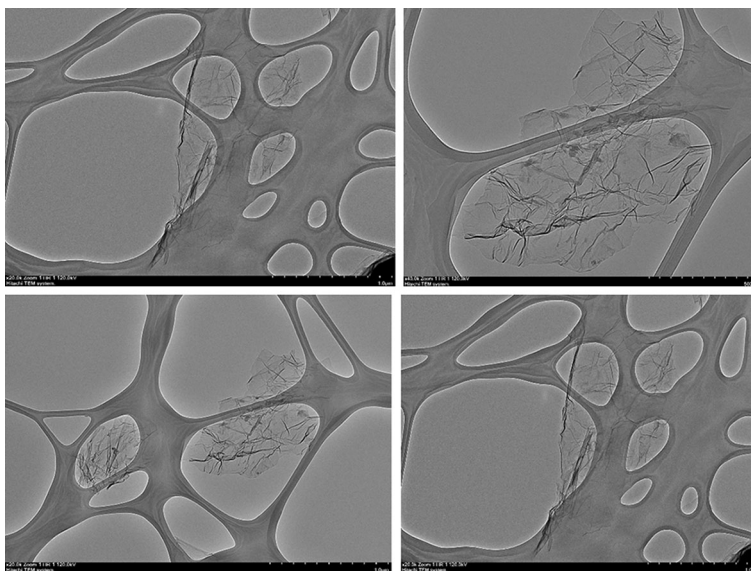
The appearance of two bands at 834 and 1082  $\text{cm}^{-1}$  verified the existence of epoxy groups of PEG chain

Fig. 1 Schematic illustration of the functionalized of graphene with PEG





**Fig. 3** High-resolution TEM images of graphene



**Fig. 4** FTIR spectra of pristine graphene and PEG-graphene

[24, 39]. Two new bands appeared at 1416 and 2934  $\text{cm}^{-1}$  are related to the symmetric and antisymmetric C–H in  $\text{CH}_2$  groups of PEG chains. The existence of carboxyl groups was recognized by a peak appeared at 3270  $\text{cm}^{-1}$ . This peak is characterized by C=O stretching vibrations from carboxyl and carbonyl groups of graphene [39].

These evidences demonstrated that PEG was incorporated into carbon skeleton during the functionalization of pristine graphene nanosheets. These evidences demonstrate that the graphene nanosheets have been successfully functionalized with pristine to become PEG-graphene [23]. As mentioned earlier, covalent functionalization is performed via an electrophilic addition reaction between graphene and the PEG chain under microwave irradiation, which was confirmed by FTIR spectroscopy.

### Raman spectroscopy

Raman spectroscopy is a vibrational method being very sensitive to geometric structure and bonding within molecules. Even slight differences in geometric structure cause considerable differences in the observed Raman spectrum of a molecule. This sensitivity to geometric structure is very helpful for studying the different allotropes of carbon where the different forms vary only in the relative position of their carbon atoms and the nature of their bonding to one another. In fact, Raman has emerged as an essential tool in laboratories performing research into the nascent field of carbon nanomaterials.

Functional groups were identified and characterized on the surface of PEG-functionalized graphene by Raman spectroscopy. Raman spectroscopy is a strong tool to characterize the degree of nanostructure functionalization.

The ratio of the intensities of the D band to the G band ( $I_D/I_G$ ) is regarded as the amount of disordered carbon ( $\text{sp}^3$ -hybridized carbon) relative to graphitic carbon ( $\text{sp}^2$ -hybridized carbon). In studies on the functionalization of carbon nanostructures, the higher intensity ratio of  $I_D/I_G$  demonstrates the higher disruption of aromatic  $\pi$ - $\pi$  electrons, suggesting the partial damage of graphitic carbon created by expansion and edge functionalization [20, 37].

As can be seen in Fig. 5, in the Raman spectrum of pristine graphene nanosheets, the G band is at 1567  $\text{cm}^{-1}$ , the intensity of the D band is at 1346  $\text{cm}^{-1}$  and the 2D band is at 2685  $\text{cm}^{-1}$ . The Raman spectrum of PEG-graphene is shown in Fig. 5 in which D band is observed at 1349  $\text{cm}^{-1}$ , and there are relatively strong G and 2D bands at 1581 and 2708  $\text{cm}^{-1}$ , respectively.

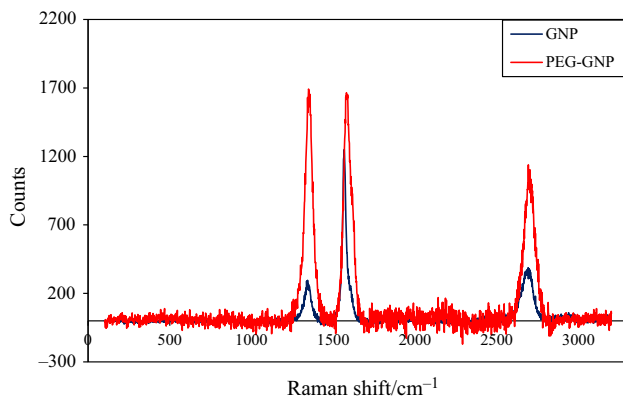


**Fig. 5** Raman spectra of pristine graphene and PEG-graphene

The Raman results powerfully indicate a significant increase in the  $I_D/I_G$  ratio of pristine graphene compared to that of PEG-graphene from 0.2 to 1.02, suggesting the process of functionalization is performed appropriately.

As mentioned above and according to Fig. 5,  $I_D/I_G$  ratios of PEG-graphene were much greater than those of pristine graphite confirming the successful functionalization through an electrophilic addition reaction under microwave irradiation [20, 37].

## Experimental setup

A schematic diagram of the experimental pool boiling facility is exhibited in Fig. 6, which was designed to run pool boiling experiments for boiling heat transfer and CHF under atmospheric pressure. The setup involved four main components (a) boiling vessel, (b) power and monitoring system control, (c) section of samples test (boiling surface) and (d) heating section.

Boiling vessel was a 300 mm × 150 mm × 150 mm rectangular vessel made of Pyrex which had sufficient thermal resistance against high-temperature shocks.

It has four windows which allows the test to be observed as it progresses, a place where the test section can be positioned horizontally so that the boiling phenomena occurring on the test heater could be seen. At the bottom section of vessel, a perforated hole has been provided, in which a main heater (stainless steel heater block) is mounted. A small layer of Teflon was employed for the prevention of any liquid leakage and heat loss between block heater and the hole.

Heating section had a S.S. heater block with four cartridge heaters provided heat to the test section, and each cartridge heaters had individual maximum heating power of 700 W and with height of 90 mm. A reflux condenser was mounted at the top of the main pool chamber for the evaporation of the deionized water to be prevented.

Since Teflon and rock wool were used to insulate the S.S. block, which had a very small thermal conductivity of  $0.03\text{--}0.25\text{ W m}^{-1}\text{ K}^{-2}$ , the heat transfer through the block could be simplified as a one-dimensional steady-state conduction heat transfer problem. Later, during the experiment when the temperatures of thermocouples 4 and 5 were equal, this was confirmed.

Test samples section was located on top of a cylindrical S.S. block with 40 mm diameter at the bottom of the pool (vessel), as indicated in Figs. 6 and 7.

The test surface was polished to a roughness of less than  $1\text{ }\mu\text{m}$  (a mirror-polished). The test samples were heated by conduction from the heating section, which consisted of four cartridge heaters.

In order to minimize heat loss, all parts of the experimental setup and the surrounding parts of the S.S. block were insulated using Teflon and rock wool.

During the experiment, the bulk temperature was retained at  $100\text{ }^\circ\text{C}$  using feedback control of the auxiliary heaters according to the thermocouple readings. In other words, first the entire boiling vessel was heated by an external auxiliary heater surrounding the vessel prior the start of the boiling experiment to ensure that the bulk test fluid was maintained at a temperature below the boiling temperature. Power and monitoring system control contains the following equipment.

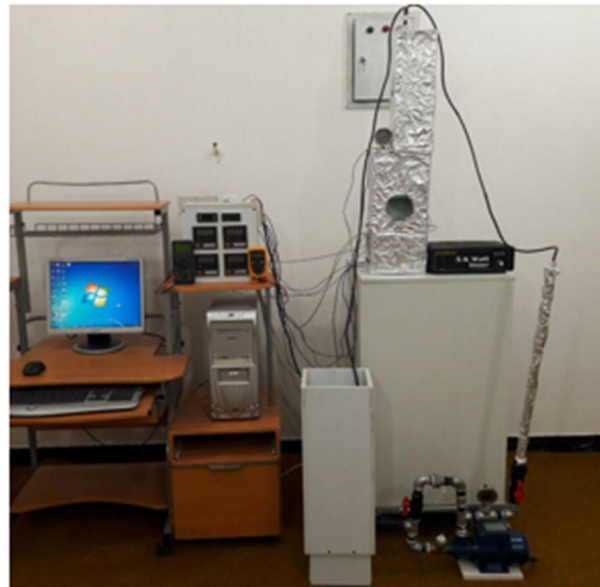
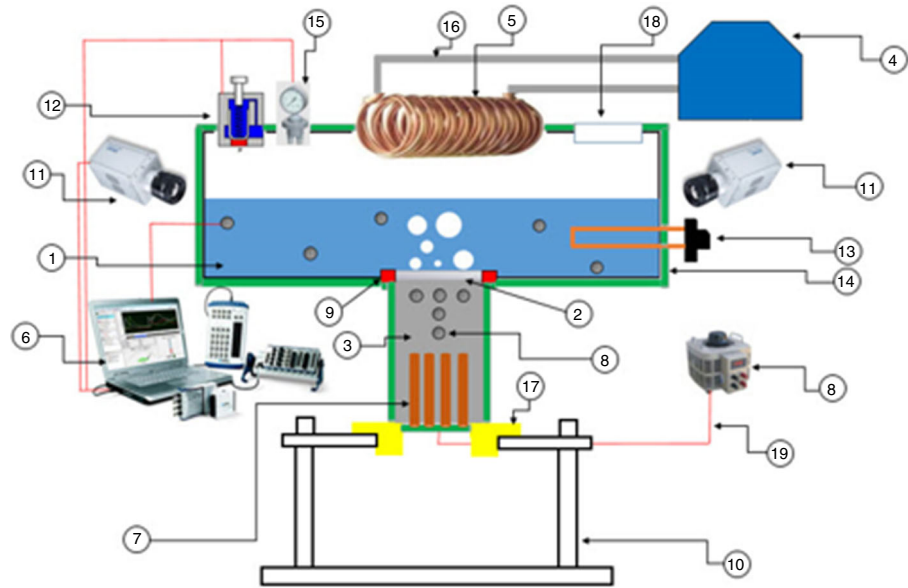
Five  $K$ -type thermocouples ( $T_1$ ,  $T_2$ ,  $T_3$ ,  $T_4$  and  $T_5$ ) were embedded in the S.S. cylinder at the top of the assembly (Fig. 7) to monitor the temperature. The distance between the thermocouples and the thermal conductivity of S.S. heater block are known, and by measuring the temperature, the heat flux through the test surface ( $T_{\text{wall}}$ ) could be calculated by Fourier law. The surface temperature was obtained by extrapolation. In order to check local temperature four thermocouples were positioned at different points in the fluid.

A data acquisition system was employed to collect data on the heat flux and thermocouples temperatures (Datalog-CUP110). A DC power supply with a contact voltage regulator of 20 kW (OMGV20 K-1P) was employed to indicate different input powers and adjust the temperature of the heater surface. The boiling apparatus involving vessel, condenser and all pipes were thoroughly insulated to decrease uncertainty in the setup.

A condenser with a copper tube and a safety valve was placed at the top of the section of vessel to control the pressure and condense the vapor into liquid.

## Data reduction and uncertainty

In this type of experiments, it is very important to estimate uncertainty in the measurement of heat flux and heat transfer coefficient. In the present study, the uncertainties

**Fig. 6** Schematic of pool boiling setup

Part No.	Name
1	Boiling vessel
2	Boiling surface
3	S.S heater block
4	Cooling chamber
5	Condenser
6	Data acquisition
7	Cartridge heaters
8	Thermocouples
9	Holder boiling surface
10	Main support of vessel
11	High speed camera
12	Relief valve
13	Auxiliary heater
14	Insulation material
15	Pressure gauge
16	Condenser in/out pipes
17	Ceramic insulation and holder
18	Fluid inlet
19	Electrical/data cables
20	Dc power supply

were calculated by Jaikumar et al. method [31]. Thermal conductivity of stainless steel, thermocouple calibration and the distance between thermocouples all contributed to the uncertainty calculations. The method of partial sums was employed to calculate the uncertainty.

In this research, a heat loss study was carried out to ensure that the heat is transferred by 1D conduction to the test surface. According to Fourier law of heat conduction, it is expected that the temperature profile across the test section is linear. Also, since the temperatures of thermocouples 4 and 5 are the same as the temperature of thermocouple 3, this result is inferred.

Figure 8 indicates temperature distribution for heat flux 114, 393 and 519 kW m<sup>-2</sup> plotted between  $T_3$  and  $T_1$  for test surface which depicted linear progression with R

squared value close to 1 which ensured minimal heat loss during the experimental process.

Two main errors arising during experimentation are bias errors and precision errors. The bias errors are resulted from calibration, and precision errors are owing to sensitivity of the testing devices. Collectively, the errors owing to bias and precision can be expressed as,

$$U_y = \sqrt{B_y^2 + P_y^2} \quad (1)$$

where  $U_y$  is the uncertainty or error,  $B_y$  is the bias error, and  $P_y$  is the precision error. The parameters that contribute to errors are thermocouple calibrations, thermal conductivity of stainless steel and the distance between the thermocouple spacing on the test chip. The calibration of

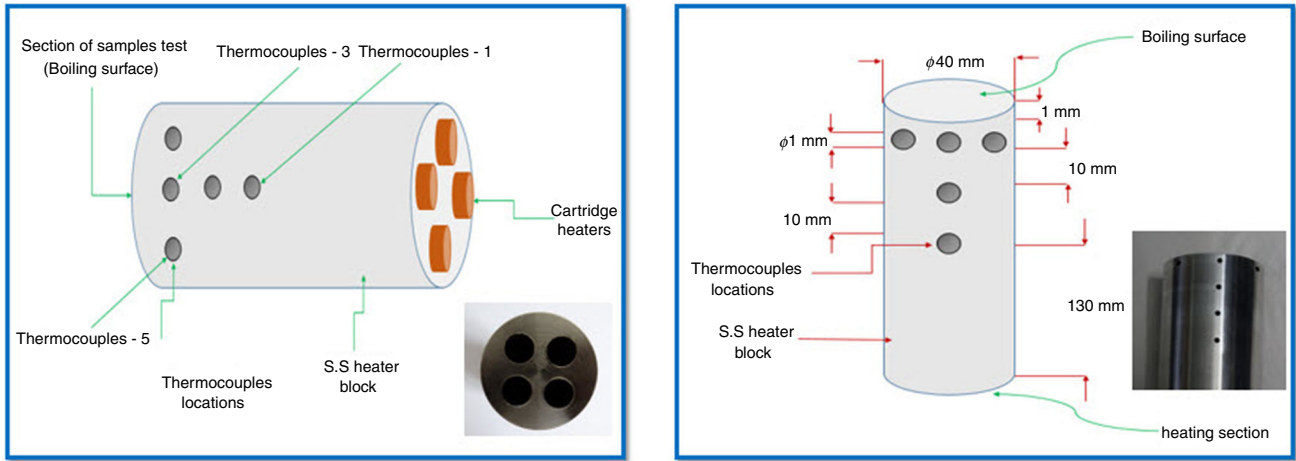


Fig. 7 Details on geometrical properties of heater surface and heater block

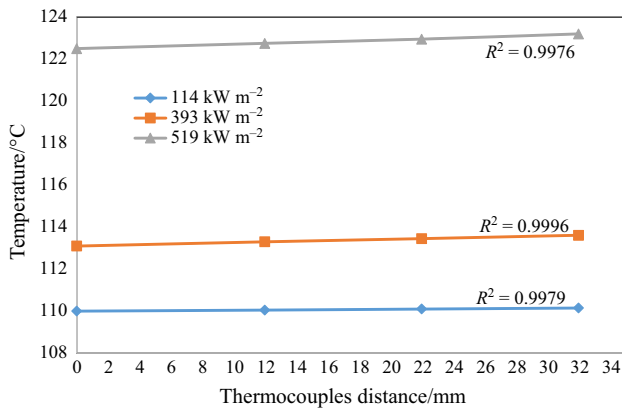


Fig. 8 Temperature distribution at different heat fluxes measured between  $T_3$  and  $T_1$

thermocouples was conducted, and its precision error was calculated statistically as  $\pm 0.01$  °C.

Since measuring temperature directly at the heated surface can influence on the bubble growth process because of the variation in the heated surface geometry, the temperature of the heated surface ( $T_w$ ) was calculated by the heater temperature ( $T_{th}$ ) measured using the thermocouple and the heat flux ( $q''$ ) created by the experimental heater [40]. Assuming that the heat flux is transferred in the axial direction, the temperature of the heated surface can be calculated by a one-dimensional heat conduction equation, as indicated in Eqs. (2) or (4)

$$q'' = -k \frac{dT}{dx} \tag{2}$$

The temperature gradient  $dT/dx$  was computed by the three-point backward Taylor's series approximation.

$$\frac{dT}{dx} = \frac{3T_1 - 4T_2 + T_3}{2\Delta x} \tag{3}$$

where  $T_1$ ;  $T_2$ ;  $T_3$  are the temperatures corresponding to the top, middle and bottom of the test chip studied, respectively. The boiling surface temperature was calculated using Eq. (2) and is given by,

$$T_w = T_3 - \frac{x_1}{k} q'' \tag{4}$$

where  $T_w$  is the boiling surface temperature and  $x_1$  is the distance between the boiling surface and  $T_3$ ;  $x_1$  is equal to 1 mm for all the test surfaces (see Fig. 7).

$q''$  is the heat flux. The heat flux ( $q''$ ) can be obtained by Eq. (4) as follows:

$$q'' = \frac{V_{heater} I_{circuit}}{A_{sur}} \tag{5}$$

where  $V_{heater}$ ,  $I_{circuit}$  and  $A_{sur}$  are the voltage and electric current of the experimental heater, and surface area of the heated surface, respectively.

The test section heater has been insulated with Teflon and rock wool; thus, one-dimensional conduction heat transfer is the dominant heat transfer mechanism. The heat fluxes estimated from Eq. (4) and that of calculated by Eq. (5) were compared to indicate the amount of heat loss along the heater block [41]. As mentioned, the extrapolation of the surface temperature of test surface of heater is necessary for calculating the pool boiling heat transfer coefficient. Indeed, the measure for thermal performance of a nanofluid is the pool boiling heat transfer coefficient, which can be obtained by Eq. (6):

$$h = \frac{q''}{T_w - T_{sat}} \tag{6}$$

where  $T_w$  and  $T_{sat}$  are temperature at the heated surface and saturation temperature, and the uncertainties of the heat



flux and BHTC (boiling heat transfer coefficient) can be calculated by Eqs. (6) and (7), respectively.

$$\frac{\Delta q''}{q''} = \sqrt{\left(\frac{\Delta V}{V_{\max}}\right)^2 + \left(\frac{\Delta I}{I_{\max}}\right)^2 + \left(\frac{\Delta A}{A}\right)^2} \quad (7)$$

$$\frac{\Delta q''}{q''} = \sqrt{\left(\frac{\Delta V}{q''}\right)^2 + \left(\frac{\Delta T}{T}\right)^2} \quad (8)$$

It is of note that thermocouples and multi-meter readings were carried out three times to ensure that data are reproducible. The maximum deviation associated with the measurement of location of the thermocouples was about 0.1%. Table 2 indicates the uncertainties of measurement equipment used in this study.

## Results and discussion

### Thermal conductive of nanofluids

The main reason for using nanoparticles in a conventional fluid is to enhance thermal conductivity. Since thermal conductivity of nanofluids is higher than that of base fluids, it is expected that the heat transfer characteristics of nanofluids to be higher than those of the base fluids make them more promising for heat transfer applications, particularly for pool boiling heat transfer [42].

Measuring thermal conductivity was a challenge for a long time since different methods and techniques yielded different results. So the method should be used that is able to reduce the measurement error and uncertainty as much as possible. The calculation of thermal conductivity of nanofluids can be performed either experimentally or analytically.

Some of the experimental techniques used for measuring thermal conductivity of nanofluids include transient hot wire method, steady-state parallel plate technique and temperature oscillation technique are.

It is worth mentioning that it was the found that the experimental results were much higher than the results of theoretical models. This proves that a new heat transport mechanism in nanofluids exists [32].

**Table 2** Uncertainty of measurement parameters

Parameter	Unit	Uncertainty value
Temperature ( $T$ )	K	$\pm 0.1$
Voltage ( $V$ )	V	$\pm 0.1\%$ of reading
Distance ( $L$ )	m	0.001
Current ( $A$ )	A	$\pm 0.1\%$ of reading
Bulk temperature ( $T$ )	K	$\pm 0.1$

In this study, a transient short hot wire technique was employed to measure thermal conductivities of nanofluids from 20 to 60 °C by a KD2 Pro device (Decagon devices, Inc., USA), because of all the techniques, the transient hot wire technique is most commonly used by researchers. This is a fast and accurate technique for measuring thermal conductivity of nanofluid [43, 44].

Before starting the test for nanofluids and measuring its parameters, deionized water as a test fluid was used for calibrating the experimental setup. The sample nanofluid was placed in a glass container, and it was kept inside a circulating system of constant temperature deionized water bath (Make: JEIO Tech, Korea, capacity: 5 L, temperature range:  $- 25$  °C to  $+ 150$  °C, temperature stability:  $\pm 0.05/0.09$  °C).

For measuring thermal conductivity, the vessel containing the tested sample was taken in the bath and a thermocouple inside the vessel was employed to monitor the sample temperature. It is of note that thermal conductivity for each nanofluid with different volume fractions of graphene nanoplatelets and at temperatures between 10 and 70 °C is measured five times and the average of the five data points is reported.

The percentage values displayed are according to the expression  $100(k_{\text{nf}} - k_f)/k_f$ , where ' $k_{\text{nf}}$ ' is the thermal conductivity of nanofluid and ' $k_f$ ' is the thermal conductivity of water.

### Thermal conductive measurement

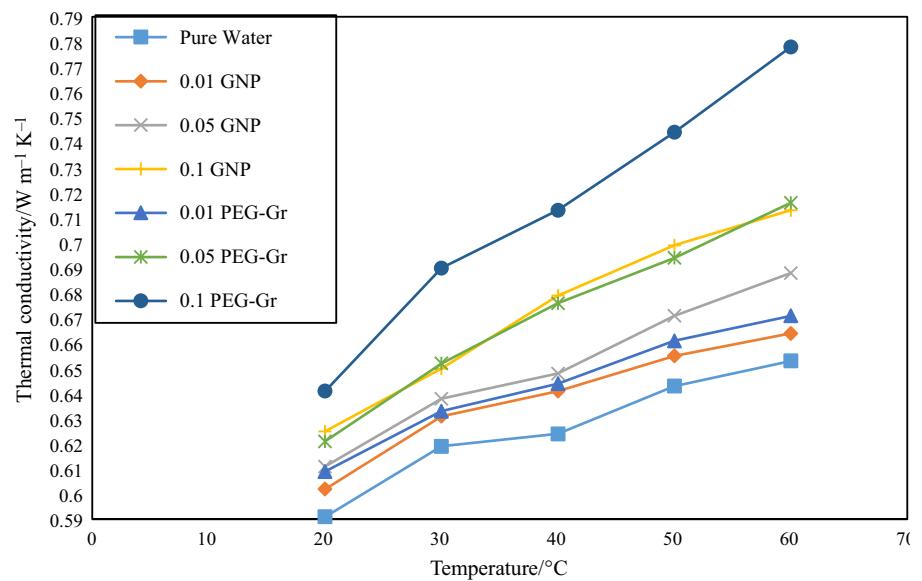
The effect of operating temperature on thermal conductivity of nanofluids should be considered in the design of such equipment. So it is very important for practical heat transfer applications to perform a clear study on the temperature-dependent thermal conductivity of nanofluids. Generally, thermal conductivity of nanofluids is more sensitive to temperature than base fluid [45–47]. Experiments on nanofluids yielded a variety of different results. In the majority of cases, thermal conductivity of nanofluids increases with the enhancement in temperature.

Thermal conductivity of graphene/deionized water nanofluids as a function of particle mass concentration and temperature is shown in Fig. 9. The results demonstrate that with the increase in nanofluid temperature and particle mass fraction, thermal conductivity of nanofluids increases significantly.

As can be seen in Fig. 9, with the increase in temperature, thermal conductivity of deionized water (DW) and all concentrations of functionalized and non-functionalized graphene nanofluids increase.

The experimental results clearly demonstrate that thermal conductivity of graphene nanofluid system depends on both mass fraction (%) and temperature.

**Fig. 9** Thermal conductivity of graphene/DW nanofluids as a function of temperature and mass% fraction



By raising temperature from 20 to 60 °C and concentration from 0.01 to 0.1 mass%, thermal conductivity increased for all samples. It is of note that the improvement for PEG-functionalized graphene nanofluids was much more than non-functionalized ones. This finding proves that graphene nanofluids are capable of increasing thermal conductivity with the increase in temperature and concentration (up to 0.1 mass%). This behavior can be explained by Brownian motion which caused the bigger particles to be agglomerated at high temperatures [48]. Since more functional groups are present in higher concentration samples, more destruction of functional groups by increasing temperature can be another reason [49]. So, by partial elimination of functional groups from graphene, distribution of nanosheets is reduced, while the increase in conduction is low. Thermal conductivity results of the samples are consistent with those of Baby et al. [50] and Ghozatloo et al. [23] and many other researchers [16, 22, 51].

Also Fig. 12 showed that first, graphene functionalized with polyethylene glycol (0.1 mass%) had higher thermal conductivity than other samples. Second, the results indicated that thermal conductivity of PEG-graphene nanofluid (0.1 mass%) had the highest percentage of change with the increase in the nanofluid temperature (about 20%). Third, at the maximum operating temperature (60 °C), PEG-graphene nanofluid (0.1 mass%) had the highest percentage of change in thermal conductivity compared to deionized water (about 19.1%), and at the same concentration, the percentage of change in graphene nanofluids without functionalization was twice in comparison with deionized water. Figure 10 indicates thermal conductivity ratio as a function of temperature.

As can be observed in Fig. 10, it is obvious that the above items can be deduced. For example, the thermal conductivity value of graphene nanofluid without functionalization (0.1 mass%) was approximately equal to that of PEG-graphene nanofluid (0.05 mass%), while the concentration of graphene nanofluid without functionalization (0.1 mass%) was twice that of PEG-graphene nanofluid (0.05 mass%).

Also according to previous researchers, for example Ramesh et al. [52], thermal conductivity of deionized water increases by 9% when 0.1 mass% functionalized carbon nanotubes (CNT) powders are added. In this study, thermal conductivity of PEG-graphene-deionized water nanofluid (0.1 mass%) was 2.13 times higher and equal to 113% compared to the CNT thermal conductivity.

### Pool boiling

It is important to know that increased thermal conductivity of nanofluids only provides a 'necessary' condition for using such fluids in cooling application and is not a sufficient condition. The real worth of such fluids also will depend on its boiling characteristics under different conditions [53].

Since nanofluids have a higher thermal conductivity than base fluids, it is expected that the heat transfer characteristics of nanofluids to be higher than those of base fluids make them more promising for heat transfer applications, particularly for pool boiling heat transfer.

Boiling is a common but a very efficient mode of heat transfers in which liquid-phase changes to vapor phase over a hot surface taking away a high amount of thermal energy with a small temperature difference.

**Fig. 10** Thermal conductivity ratio of graphene/DW nanofluids as a function of temperature and mass fraction (%)

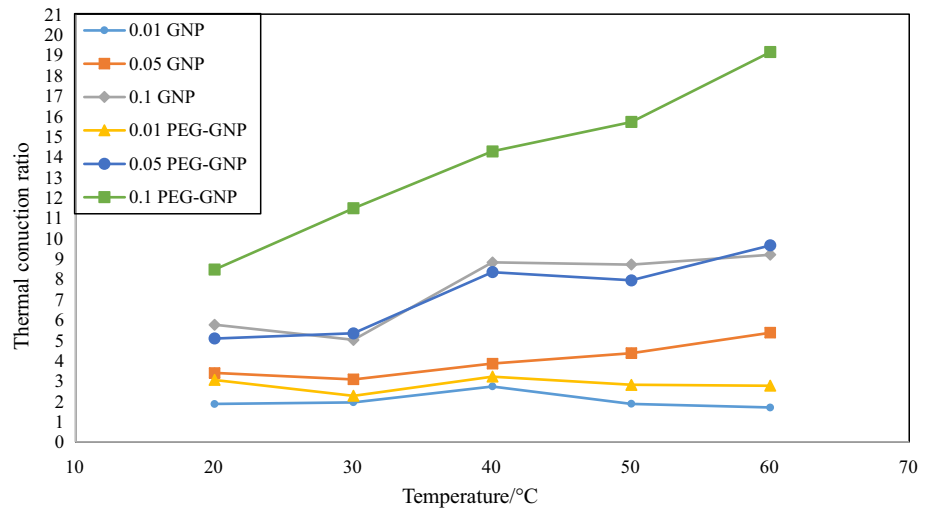
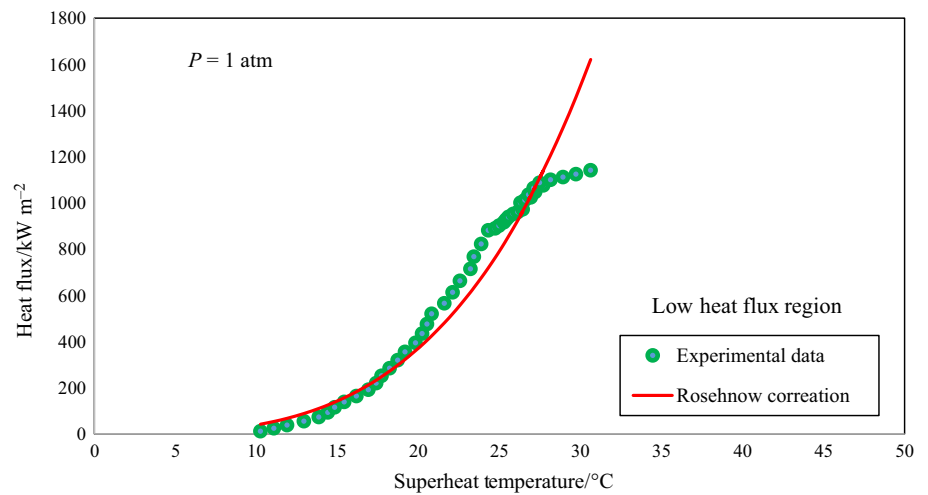


**Fig. 11** Comparison heat flux as a function of difference superheat temperatures for experimental data with Rohsenow's correlation of the deionized water



To inspect the reliability of the apparatus, the experimental results for the nucleate pool boiling heat transfer of deionized water were compared to the data predicted by well-known correlations. Rohsenow [54] correlation was suggested for predicting the nucleate pool boiling heat transfer.

This equation assumes that the main heat transfer mechanism in nucleate boiling conditions is the convection strength due to turbulence from bubble vapor (for this equation the fluid is in saturated conditions).

Moreover, the CHF of deionized water was calculated by Zuber correlation [55]. Figure 11 indicates the experimental results compared to Rohsenow correlation for the boiling curve, and to Zuber correlation for CHF. The experimental results of the boiling curve according to the superheat on the surface were in agreement with the Rohsenow correlation. It is easy to see that the present results are in good agreement with the predictions of Rohsenow [54] and Zuber [55]. Mean absolute percentage error (MAPE) for heat fluxes was about 14.26%. As can be

seen in Fig. 11, it can be stated that at lower heat flux, higher MAPE was seen (about 19%), while for high heat flux and moderate heat flux conditions, lower MAPE was registered (about 11%).

To conduct the tests and to obtain CHF it is required to obtain a high heat flux, which is a relatively considerable technical challenge. In fact, the CHF for atmospheric conditions, deionized water and a clean heating surface is about 700–1400 kW m<sup>-2</sup> and based on the literature with a nanofluid 2000 kW m<sup>-2</sup> or even higher can be achieved. To this purpose, some authors suggest a direct electric heating system through a wire or surface where the calculation of heat flux and wall temperature is performed by the power injected and change in electrical resistance (as function of temperature), respectively [28]. In this case, the samples are often broken when the CHF is obtained because the sample temperature increases rapidly, which exceeds the limits of its constituent materials.

Our experimental setup follows the method explained by Mourgues et al. [28]. We employ an indirect heating

system in which the sample surface is heated by thermal conduction. In fact, the heat generated by the electric cartridges inserted into a thermal conductor body (S.S. 316) drives the heat to the sample. This method has also been suggested by other authors. In this case, heat flux and wall temperature are calculated by Fourier's law. There are two main advantages for this method. Firstly, the complete evolution of the heat flux from nucleate boiling to well-established film regime can be obtained, so the CHF will be clearly known, and secondly, this system prevents sample breakage and/or damage [28].

The experiments were performed to clarify the pool boiling of graphene nanofluid. Graphene nanoplatelets were dispersed in deionized water at the concentrations of 0.01, 0.05 and 0.1%. Figure 12 indicates the experimental results of heat flux versus superheat temperature for both graphene nanofluids and PEG-graphene nanofluids at different concentrations of nanoparticle and base fluid.

As indicated in Fig. 12, for all concentrations the boiling heat transfer performance of graphene nanofluids was higher than that of deionized water. At the maximum level (0.10 mass% PEG-graphene), the critical heat flux of PEG-graphene increased 72% compared to deionized water. The boiling performances of the 0.01, 0.05 and 0.10 mass% graphene nanofluids improved with the increase in concentration. At the same superheat temperature, the observed heat flux increased for graphene nanofluids compared to deionized water, especially for functionalized graphene nanofluids. On the other hand, CHF of the functionalized graphene nanofluids was higher than that of graphene nanofluids and deionized water at the same concentration.

Figure 13 indicates the experimentally quantified pool boiling heat transfer coefficient of graphene nanofluids at different mass concentrations. As predicted, by increasing the heat flux applied to the boiling surface, the heat transfer coefficient increases significantly. Indeed, an increase in heat flux enhances the rate of bubble formation and the rate

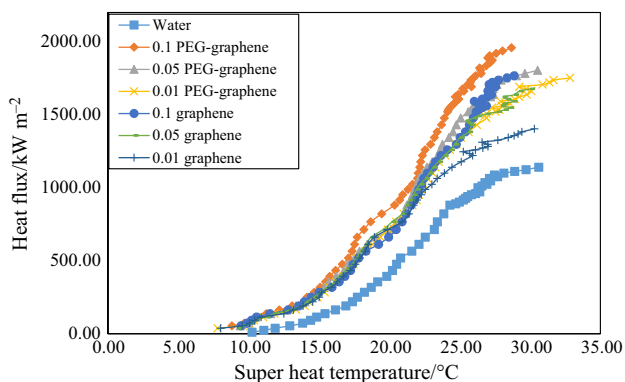


**Fig. 12** Heat flux in boiling conditions versus superheat temperature and critical heat fluxes values of graphene-deionized water nanofluids

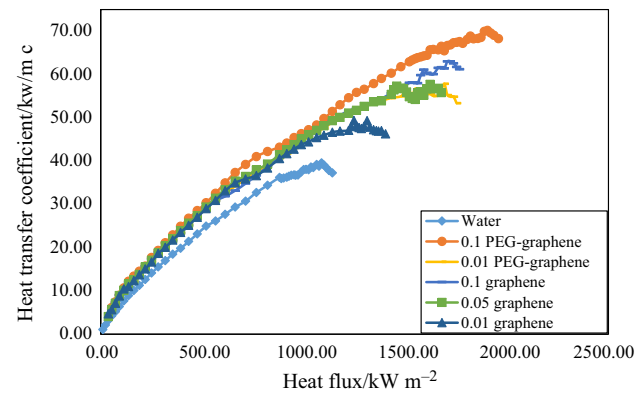


**Fig. 13** Boiling HTC versus heat flux for graphene-DW nanofluids, PEG-graphene nanofluids and DW

of heat transfer on the surface leading the local agitation, bubble interaction and micro/macro-convection streams around the bubbles to be intensified too.

Also, by increasing the mass concentration of graphene nanofluids, pool boiling heat transfer coefficient enhances, while the rate of increase in heat transfer coefficient in the low heat flux region is lower than that of reported in moderate and high heat flux regions. As can be observed, the heat transfer coefficient for graphene nanofluids is higher than that of deionized water. The reason can be attributed to the internal thermal conductivity of graphene nanofluids, Brownian motion of graphene inside the bulk of nanofluids and thermal diffusion from the surface to the bulk of nanofluids (thermophoresis phenomenon).

As can be seen in Fig. 13, by increasing heat flux the gap between the heat transfer coefficient of graphene/DW nanofluids as a non-covalent nanofluid and that of deionized water increased.

It is clear that convective heat transfer is the main parameter in the pool boiling heat transfer. According to multiple studies, the main mechanism in the pool boiling heat transfer is free convection before reaching to CHF. It is implied that a fluid can circulate in a closed loop with no need for any pump or an external force [30]. Surprisingly, the results supported that the pool boiling HTC (heat transfer coefficient) of covalent nanofluids is higher than that of non-covalent nanofluids as well as the deionized water. Consistent with our results, the method of functionalization and the kind of functional group added to the surface of graphene affected on the boiling heat transfer coefficient [30].

Figure 14 shows the CHF enhancement, given the definition of the ratio of nanofluid CHF (at various concentrations) to deionized water CHF. The results indicated that the CHF ratio of nanofluid was higher than that of the base fluid and increased by raising concentration. This means that the CHF increased strongly as the concentration of



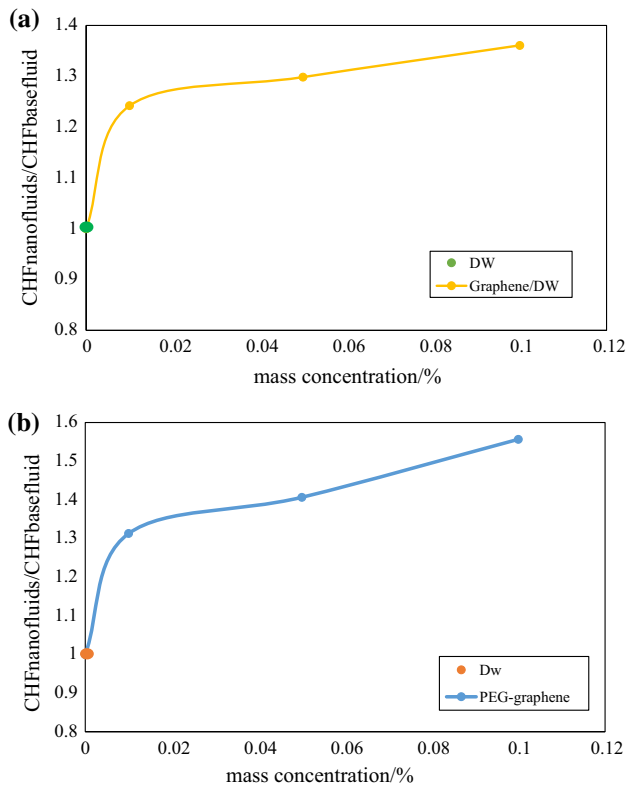


**Fig. 14** CHF enhancement defined as the ratio of **a** graphene nanofluids and **b** PEG-graphene nanofluids CHF compare deionized water CHF as a function of the mass concentration

graphene increased from zero that is shown in Fig. 14a, and became saturated at concentrations more than 0.01 vol%. This is in agreement with previous reports on CHF phenomenon with graphene nanofluid [28, 29, 56, 57]. In a similar manner, the CHF increased tremendously with increased PEG-graphene concentration, as indicated in Fig. 14b. However, the improvement was more than CHF of the graphene nanofluid. Maximum CHF of the nanofluid was 72% greater than that of DW, and maximum CHF ratio was 1.56 occurred at 0.1 mass% PEG-graphene.

## Conclusions

We studied the pool boiling heat transfer of graphene nanofluids performed on a flat heater surface under the atmospheric pressure. This study also examined thermal conductivity behavior of nanofluids based on graphene and functionalized graphene (PEG-graphene). Pool boiling heat transfer properties such as boiling HTC, CHF, influence of heat flux and nanoparticle mass fraction on BHT, effective thermal conductivities of graphene nanofluids have been measured and discussed.

The effective thermal conductivities were determined versus temperature for different concentrations of

graphene. The results demonstrated that there was an increase in thermal conductivity in heat transfer for graphene nanofluids dispersed in deionized water. By increasing graphene concentration and temperature, the thermal conductivity improved.

Thermal conductivity improvement was 9 and 19% for graphene nanofluid and PEG-graphene nanofluid, respectively (mass percentage of 0.1%) at 60 °C.

The results indicated that at all concentrations PEG-graphene nanofluids (0.01, 0.05, 0.1 mass%) had sufficient dispersion and fewer tendencies for agglomeration and precipitation compared to graphene without functionalization. Likewise, the values of CHF and HTC improved for all test cases 72 and 77%, respectively. Moreover, analysis of the results demonstrated that the critical heat flux (CHF) of nanofluids when boiled over a stainless steel flat plate test section enhances as the concentration of graphene nanoparticles in the base fluid increases. The highest enhancement compared to deionized water has been found to be 45 and 72% for functionalized graphene with PEG.

At the same heat flux, the heater surface temperature of nanofluids was lower than that of the base fluid, especially when functionalized nanofluids were used.

Eventually, thermal conductivity, viscosity, CHF and HTC of graphene nanofluids are obviously dependent on functional groups. Thermophysical characteristics of functional groups could change thermal performance, and as mentioned above, the value for functionalized graphene nanofluids was higher than that of non-functionalized graphene nanofluids were.

**Acknowledgements** The authors gratefully acknowledge the Department of Chemical Engineering, Mahshahr Branch, Islamic Azad University, for the support to this project.

## References

1. Ahn HS, Kim JM, Park C, Jang J-W, Lee JS, Kim H, et al. A novel role of three dimensional graphene foam to prevent heater failure during boiling. *Sci Rep.* 2013;3:1960.
2. Soleymaniha M, Felts JR. Design of a heated micro-cantilever optimized for thermo-capillary driven printing of molten polymer nanostructures. *Int J Heat Mass Transf.* 2016;101:166–74.
3. Zhang C, Cheng P. Mesoscale simulations of boiling curves and boiling hysteresis under constant wall temperature and constant heat flux conditions. *Int J Heat Mass Transf.* 2017;110:319–29.
4. Choi SU, Eastman JA. Enhancing thermal conductivity of fluids with nanoparticles. Illinois: Argonne National Lab.; 1995.
5. Amiri A, Shanbedi M, Dashti H. Thermophysical and rheological properties of water-based graphene quantum dots nanofluids. *Journal of the Taiwan Institute of Chemical Engineers.* 2017;76:132–40.
6. Amiri A, Shanbedi M, Ahmadi G, Rozali S. Transformer oils-based graphene quantum dots nanofluid as a new generation of highly conductive and stable coolant. *Int Commun Heat Mass Transfer.* 2017;83:40–7.

7. Salimi-Yasar H, Heris SZ, Shanbedi M, Amiri A, Kameli A. Experimental investigation of thermal properties of cutting fluid using soluble oil-based TiO<sub>2</sub> nanofluid. *Powder Technol.* 2017;310:213–20.
8. Amiri A, Shanbedi M, Rafieerad A, Rashidi MM, Zaharinie T, Zubir MNM, et al. Functionalization and exfoliation of graphite into mono layer graphene for improved heat dissipation. *Journal of the Taiwan Institute of Chemical Engineers.* 2017;71:480–93.
9. Imani-Mofrad P, Saeed ZH, Shanbedi M. Experimental investigation of filled bed effect on the thermal performance of a wet cooling tower by using ZnO/water nanofluid. *Energy Convers Manag.* 2016;127:199–207.
10. Hosseini-pour E, Heris SZ, Shanbedi M. Experimental investigation of pressure drop and heat transfer performance of amino acid-functionalized MWCNT in the circular tube. *J Therm Anal Calorim.* 2016;124(1):205–14.
11. Shanbedi M, Heris SZ, Amiri A, Hosseini-pour E, Eshghi H, Kazi S. Synthesis of aspartic acid-treated multi-walled carbon nanotubes based water coolant and experimental investigation of thermal and hydrodynamic properties in circular tube. *Energy Convers Manag.* 2015;105:1366–76.
12. Hemmat Esfe M, Saedodin S. Turbulent forced convection heat transfer and thermophysical properties of Mgo–water nanofluid with consideration of different nanoparticles diameter, an empirical study. *J Therm Anal Calorim.* 2015;119(2):1205–13. <https://doi.org/10.1007/s10973-014-4197-1>.
13. Raei B, Shahraki F, Jamialahmadi M, Peyghambarzadeh SM. Experimental study on the heat transfer and flow properties of  $\gamma$ -Al<sub>2</sub>O<sub>3</sub>/water nanofluid in a double-tube heat exchanger. *J Therm Anal Calorim.* 2017;127(3):2561–75. <https://doi.org/10.1007/s10973-016-5868-x>.
14. Arabpour A, Karimipour A, Toghraie D. The study of heat transfer and laminar flow of kerosene/multi-walled carbon nanotubes (MWCNTs) nanofluid in the microchannel heat sink with slip boundary condition. *J Therm Anal Calorim.* 2017. <https://doi.org/10.1007/s10973-017-6649-x>.
15. Hosseinzadeh M, Heris SZ, Beheshti A, Shanbedi M. Convective heat transfer and friction factor of aqueous Fe<sub>3</sub>O<sub>4</sub> nanofluid flow under laminar regime. *J Therm Anal Calorim.* 2016;124(2):827–38. <https://doi.org/10.1007/s10973-015-5113-z>.
16. Amiri A, Zubir MNM, Dimiev AM, Teng KH, Shanbedi M, Kazi SN, et al. Facile, environmentally friendly, cost effective and scalable production of few-layered graphene. *Chem Eng J.* 2017;326:1105–15. <https://doi.org/10.1016/j.cej.2017.06.046>.
17. Shazali SS, Amiri A, Zubir MNM, Rozali S, Zabri MZ, Sabri MFM, et al. Investigation of the thermophysical properties and stability performance of non-covalently functionalized graphene nanoplatelets with Pluronic P-123 in different solvents. *Mater Chem Phys.* 2018;206:94–102.
18. Geim AK, Novoselov KS. The rise of graphene. *Nat Mater.* 2007;6(3):183–91.
19. Li X, Cai W, An J, Kim S, Nah J, Yang D, et al. Large-area synthesis of high-quality and uniform graphene films on copper foils. *Science.* 2009;324(5932):1312–4.
20. Amiri A, Shanbedi M, Ahmadi G, Eshghi H, Kazi S, Chew B, et al. Mass production of highly-porous graphene for high-performance supercapacitors. *Scientific reports.* 2016;6:32686.
21. Amiri A, Shanbedi M, Chew B, Kazi S, Solangi K. Toward improved engine performance with crumpled nitrogen-doped graphene based water–ethylene glycol coolant. *Chem Eng J.* 2016;289:583–95.
22. Amiri A, Ahmadi G, Shanbedi M, Etemadi M, Mohd Zubir MN, Chew BT, et al. Heat transfer enhancement of water-based highly crumpled few-layer graphene nanofluids. *RSC Advances.* 2016;6(107):105508–27. <https://doi.org/10.1039/C6RA22365F>.
23. Ghozatloo A, Shariaty-Niasar M, Rashidi AM. Preparation of nanofluids from functionalized graphene by new alkaline method and study on the thermal conductivity and stability. *Int Commun Heat Mass Transfer.* 2013;42:89–94.
24. Țucureanu V, Matei A, Avram AM. FTIR spectroscopy for carbon family study. *Crit Rev Anal Chem.* 2016;46(6):502–20.
25. Stankovich S, Dikin DA, Piner RD, Kohlhaas KA, Kleinhammes A, Jia Y, et al. Synthesis of graphene-based nanosheets via chemical reduction of exfoliated graphite oxide. *Carbon.* 2007;45(7):1558–65.
26. Mohd Zubir MN, Badarudin A, Kazi S, Nay Ming H, Sadri R, Amiri A. Investigation on the use of graphene oxide as novel surfactant for stabilizing carbon based materials. *J Dispersion Sci Technol.* 2016;37(10):1395–407.
27. Kathiravan R, Kumar R, Gupta A, Chandra R. Preparation and pool boiling characteristics of copper nanofluids over a flat plate heater. *Int J Heat Mass Transf.* 2010;53(9):1673–81.
28. Mourgues A, Hourtané V, Muller T, Caron-Charles M. Boiling behaviors and critical heat flux on a horizontal and vertical plate in saturated pool boiling with and without ZnO nanofluid. *Int J Heat Mass Transf.* 2013;57(2):595–607.
29. Kim JM, Kim T, Kim J, Kim MH, Ahn HS. Effect of a graphene oxide coating layer on critical heat flux enhancement under pool boiling. *Int J Heat Mass Transf.* 2014;77:919–27.
30. Amiri A, Shanbedi M, Amiri H, Heris SZ, Kazi SN, Chew BT, et al. Pool boiling heat transfer of CNT/water nanofluids. *Appl Therm Eng.* 2014;71(1):450–9.
31. Jaikumar A, Gupta A, Kandlikar SG, Yang C-Y, Su C-Y. Scale effects of graphene and graphene oxide coatings on pool boiling enhancement mechanisms. *Int J Heat Mass Transf.* 2017;109:357–66.
32. Kamatchi R, Venkatachalapathy S. Parametric study of pool boiling heat transfer with nanofluids for the enhancement of critical heat flux: a review. *Int J Therm Sci.* 2015;87:228–40.
33. Hashemi M, Noie SH. Study of flow boiling heat transfer characteristics of critical heat flux using carbon nanotubes and water nanofluid. *J Therm Anal Calorim.* 2017;130(3):2199–209. <https://doi.org/10.1007/s10973-017-6661-1>.
34. Solangi K, Amiri A, Luhur M, Ghavimi SAA, Kazi S, Badarudin A, et al. Experimental investigation of heat transfer performance and frictional loss of functionalized GNP-based water coolant in a closed conduit flow. *RSC Advances.* 2016;6(6):4552–63.
35. Solangi K, Amiri A, Luhur M, Ghavimi SAA, Zubir MNM, Kazi S, et al. Experimental investigation of the propylene glycol-treated graphene nanoplatelets for the enhancement of closed conduit turbulent convective heat transfer. *Int Commun Heat Mass Transfer.* 2016;73:43–53.
36. Sarsam WS, Amiri A, Kazi S, Badarudin A. Stability and thermophysical properties of non-covalently functionalized graphene nanoplatelets nanofluids. *Energy Convers Manag.* 2016;116:101–11.
37. Amiri A, Shanbedi M, Ahmadi G, Eshghi H, Chew B, Kazi S. Microwave-assisted direct coupling of graphene nanoplatelets with poly ethylene glycol and 4-phenylazophenol molecules for preparing stable-colloidal system. *Colloids Surf, A.* 2015;487:131–41.
38. Peng X, Li Y, Zhang G, Zhang F, Fan X. Functionalization of graphene with nitrile groups by cycloaddition of tetracyanoethylene oxide. *Journal of Nanomaterials.* 2013;2013:11.
39. Hou S, Cuellari RD, Hakimi NHH, Patel K, Shah P, Gorring M et al. Amino terminated polyethylene glycol functionalized graphene and its water solubility. In: *MRS Online Proceedings Library Archive.* 2009;1205.
40. Ham J, Kim H, Shin Y, Cho H. Experimental investigation of pool boiling characteristics in Al<sub>2</sub>O<sub>3</sub> nanofluid according to surface roughness and concentration. *Int J Therm Sci.* 2017;114:86–97.

41. Sarafraz M, Kiani T, Hormozi F. Critical heat flux and pool boiling heat transfer analysis of synthesized zirconia aqueous nano-fluids. *Int Commun Heat Mass Transfer*. 2016;70:75–83.
42. Trisaksri V, Wongwises S. Nucleate pool boiling heat transfer of TiO<sub>2</sub>-R141b nanofluids. *Int J Heat Mass Transf*. 2009;52(5):1582–8.
43. Loong TT, Salleh H, editors. A review on measurement techniques of apparent thermal conductivity of nanofluids. IOP Conference Series: Materials Science and Engineering; 2017: IOP Publishing.
44. Iyahrja S, Rajadurai JS. Study of thermal conductivity enhancement of aqueous suspensions containing silver nanoparticles. *AIP Adv*. 2015;5(5):057103.
45. Shanbedi M, Heris SZ, Amiri A, Eshghi H. Synthesis of water-soluble Fe-decorated multi-walled carbon nanotubes: a study on thermo-physical properties of ferromagnetic nanofluid. *Journal of the Taiwan Institute of Chemical Engineers*. 2016;60:547–54. <https://doi.org/10.1016/j.jtice.2015.10.008>.
46. Shamaeil M, Firouzi M, Fakhari A. The effects of temperature and volume fraction on the thermal conductivity of functionalized DWCNTs/ethylene glycol nanofluid. *J Therm Anal Calorim*. 2016;126(3):1455–62. <https://doi.org/10.1007/s10973-016-5548-x>.
47. Toghraie D, Chaharsoghi VA, Afrand M. Measurement of thermal conductivity of ZnO-TiO<sub>2</sub>/EG hybrid nanofluid. *J Therm Anal Calorim*. 2016;125(1):527–35. <https://doi.org/10.1007/s10973-016-5436-4>.
48. Singh A. Thermal conductivity of nanofluids. *Defence Science Journal*. 2008;58(5):600.
49. Nasiri A, Shariaty-Niasar M, Rashidi A, Amrollahi A, Khodafarin R. Effect of dispersion method on thermal conductivity and stability of nanofluid. *Exp Thermal Fluid Sci*. 2011;35(4):717–23.
50. Baby TT, Ramaprabhu S. Investigation of thermal and electrical conductivity of graphene based nanofluids. *J Appl Phys*. 2010;108(12):124308.
51. Shanbedi M, Amiri A, Heris SZ, Eshghi H, Yarmand H. Effect of magnetic field on thermo-physical and hydrodynamic properties of different metals-decorated multi-walled carbon nanotubes-based water coolants in a closed conduit. *J Therm Anal Calorim*. 2018;131:1089–1106.
52. Ramesh G, Prabhu NK. Review of thermo-physical properties, wetting and heat transfer characteristics of nanofluids and their applicability in industrial quench heat treatment. *Nanoscale Res Lett*. 2011;6(1):334.
53. Kole M, Dey T. Thermophysical and pool boiling characteristics of ZnO-ethylene glycol nanofluids. *Int J Therm Sci*. 2012;62:61–70.
54. Rohsenow WM. A method of correlating heat transfer data for surface boiling of liquids. Cambridge: MIT Division of Industrial Cooperation; 1951.
55. Zuber N. Hydrodynamic aspects of boiling heat transfer (thesis): Ramo-Wooldridge Corp., Los Angeles, CA (United States); Univ. of California, Los Angeles, CA (United States). 1959.
56. Amiri A, Shanbedi M, AliAkbarzade MJ. The specific heat capacity, effective thermal conductivity, density, and viscosity of coolants containing carboxylic acid functionalized multi-walled carbon nanotubes. *J Dispers Sci Technol*. 2016;37:949–955.
57. Sarafraz M, Hormozi F, Silakhori M, Peyghambarzadeh S. On the fouling formation of functionalized and non-functionalized carbon nanotube nano-fluids under pool boiling condition. *Appl Therm Eng*. 2016;95:433–44.